

## Article

# Inhibition of Necroptosis in Acute Pancreatitis: Screening for RIPK1 Inhibitors

Jiaqi Yao <sup>1,2,†</sup>, Yalan Luo <sup>2,3,4,†</sup> , Xiaojun Liu <sup>1,2</sup>, Ping Wu <sup>1</sup>, Yin Wang <sup>1</sup>, Yan Liu <sup>1</sup>, Hailong Chen <sup>2,3,4,\*</sup>  and Qingping Wen <sup>1,\*</sup> 

<sup>1</sup> Department of Anesthesiology, The First Affiliated Hospital of Dalian Medical University, Dalian 116011, China

<sup>2</sup> Laboratory of Integrative Medicine, The First Affiliated Hospital of Dalian Medical University, Dalian 116044, China

<sup>3</sup> Institute (College) of Integrative Medicine, Dalian Medical University, Dalian 116011, China

<sup>4</sup> Department of General Surgery, The First Affiliated Hospital of Dalian Medical University, Dalian 116011, China

\* Correspondence: [chenhailong@dmu.edu.cn](mailto:chenhailong@dmu.edu.cn) (H.C.); [dmuwqp@163.com](mailto:dmuwqp@163.com) (Q.W.)

† These authors contributed equally to this work.

**Abstract:** This work utilizes the anthraquinone (AQ) database to identify potential inhibitors of the RIPK1 protein for developing medicines targeting AP-associated necroptosis. Screening for necroptosis-related genes that play a crucial role in AP is based on the GEO and GSEA databases. An optimum AQ for receptor-interacting protein kinase 1 (RIPK1) inhibition was virtually screened using the Discovery Studio 2019 tool, with a previously described RIPK1 inhibitor (necrostatin-1) as a reference ligand. Using LibDock and CDOCKER molecular docking, an AQ that robustly binds to RIPK1 was identified. The DOCKTHOR web server was used to calculate the ligand–receptor binding energy. The pharmacological properties and toxicity of potential AQ were evaluated using the ADME module and ProTox-II web server. The stability of ligand–receptor complexes was examined using molecular dynamics (MD) simulation. All 12 AQs showed solid binding activity to RIPK1, 5 of which were superior to necrostatin-1. Rheochrysin and Aloe-Emodin-8-O-Beta-D-Glucopyranoside (A8G) were safe RIPK1 inhibitors based on pharmacological characterization and toxicity studies. Additionally, the potential energy of the candidate AQs with RIPK1 was greater than that of the reference ligand, necrostatin-1. MD simulations also showed that the candidate AQs could bind stably to RIPK1 in the natural environment. Rheochrysin and A8G are safe and effective anthraquinones that inhibit the RIPK1 protein. This research takes a first step toward developing RIPK1 inhibitors by screening AQs that have the potential to be more effective than the reference ligand necrostatin-1.

**Keywords:** acute pancreatitis; necroptosis; RIPK1; virtual screening; anthraquinone



**Citation:** Yao, J.; Luo, Y.; Liu, X.; Wu, P.; Wang, Y.; Liu, Y.; Chen, H.; Wen, Q. Inhibition of Necroptosis in Acute Pancreatitis: Screening for RIPK1 Inhibitors. *Processes* **2022**, *10*, 2260. <https://doi.org/10.3390/pr10112260>

Academic Editors: Chi-Fai Chau, Antony Kam, Shining Loo and Simon Ming-Yuen Lee

Received: 30 September 2022

Accepted: 28 October 2022

Published: 2 November 2022

**Publisher's Note:** MDPI stays neutral with regard to jurisdictional claims in published maps and institutional affiliations.



**Copyright:** © 2022 by the authors. Licensee MDPI, Basel, Switzerland. This article is an open access article distributed under the terms and conditions of the Creative Commons Attribution (CC BY) license (<https://creativecommons.org/licenses/by/4.0/>).

## 1. Introduction

Acute pancreatitis (AP) is a common inflammatory disease in gastroenterology that is often brought on by gallstones, excessive alcohol intake, hypertriglyceridemia, and overeating [1]. AP is characterized by an abrupt start, fast development, and many complications, and its occurrence is increasing annually. Most AP patients have a mild form of the disease and recover spontaneously. However, approximately 20% of AP might progress to severe AP (SAP), prone to systemic inflammatory response syndrome and multiple organ dysfunction, with a mortality rate of 15–30% [2]. Presently, it is considered that premature activation of pancreatic enzymes by calcium overload, activation of the nuclear factor kappa B (NF- $\kappa$ B) signaling pathway, and disruption of the lysosomal-autophagic system are the initiators of AP. The premature activation of pancreatic enzymes results in the death of acinar cells, which corresponds closely with the severity of the AP [3].

Necroptosis is a different kind of programmed cell death from apoptosis and necrosis. Necroptosis is a cellular response to stress in the external environment and can be triggered by chemical or mechanical injury and inflammatory and infectious factors [4]. It is morphologically manifested by swelling of organelles and increased cell volume, most commonly resulting in cell membrane rupture. Multiple receptors may trigger necroptosis, including tumor necrosis factor receptor 1, toll-like receptor 3 (TLR3), TLR4, and interferon receptors. The receptor-interacting protein kinase 1 (RIPK1), RIPK3, and mixed-lineage kinase domain-like protein (MLKL) form the core structural domain of the necroptosis pathway [5]. PIPK1 is the initial signaling molecule in the necroptosis pathway; it induces apoptosis by activating NF- $\kappa$ B, MAPK, and caspase-8 pathways. Notably, RIPK1 is a multifunctional signaling kinase, and its activation is not a necroptosis signature. RIPK3 and MLKL are essential components of necroptosis and constitute its core. Active RIPK3 interacts with the kinase-like structural domain of MLKL, resulting in phosphorylation and activation of MLKL. Active MLKL induces cell enlargement and membrane rupture [6]. It is generally accepted that the massive release of damage-associated pattern molecules from cells after the onset of necroptosis is key to inducing increased inflammation in AP. Inhibition of necroptosis signaling might be a potential strategy for treating AP [7].

Through the principles of drug design and a suite of specialized programs, virtual screening may identify potentially beneficial novel compounds out of hundreds of thousands or even millions of molecules with known target binding abilities. Virtual screening is a crucial technique to prevent blindness in drug research and dramatically reduce the length of the medication development cycle [8]. Anthraquinone (AQ) is a class of natural compounds with carbonyl groups and belongs to the group of polycyclic aromatic hydrocarbon derivatives. AQ is widely found in higher plants, such as Liao, Rhamnaceae, Rubiaceae, and Liliaceae. Chinese herbs, such as *Rheum officinale*, *Aloe Vera*, and *Tripterygium wilfordii* contain many AQs [9]. Recent evidence demonstrates that AQs from *Rheum officinale* have significant protective effects against AP-induced pancreatic injury and extra-pancreatic organ damage. However, whether or how AQs may reduce the severity of AP by reducing necroptosis is unknown [10–13].

The GEO and GSEA databases were used to identify necroptosis-related targets that play a crucial role in AP pathogenesis. Then, virtual screening was created using the Discover studio software. The previously described RIPK1 inhibitor necrostatin-1 served as the reference ligand [14], and molecular docking using the LibDock and CDOCKER modules was utilized to evaluate the interaction between AQs and RIPK1. Using the ADME module and ProTox-II web server, the pharmacological and toxicological properties of the AQs were also evaluated. Molecular dynamics (MD) simulations were used to evaluate the stability of the ligand–receptor complexes.

## 2. Materials and Methods

### 2.1. Data Collection

GSE109227, a gene microarray associated with AP, was selected from the GEO database. Microarrays for the GSE109227 gene set were obtained from the GPL6246 platform, and a total of 11 mouse pancreatic tissues from the control and AP groups were included in the dataset. The online analysis tool GEO2R was used to screen differentially expressed genes (DEGs) at  $p < 0.05$ ,  $|\log_2\text{fold change (FC)}| > 1$  (Supplementary Materials) and map the volcanoes of DEGs. Subsequently, a total of 67 differentially expressed necroptosis-related genes (Supplementary Materials) were identified in AP via the GSEA database (<https://www.gsea-msigdb.org/gsea/index.jsp>, accessed on 10 September 2022).

### 2.2. Necroptosis-Related DEGs Identification and Construction of PPI

Identification of differentially expressed necroptosis-related genes in AP was conducted by plotting a Venn diagram. Those genes identified were imported into the STRING database (<https://stringdb.org/>, accessed on 10 September 2022), and the species was set to “Homo sapiens” to extract protein-protein interaction (PPI) information. Cytoscape

software was utilized to visualize the protein interaction information, constructing the PPI network. CytoNCA was used to analyze the centrality degree of network nodes to identify critical genes. The protein structures matching the essential genes were also obtained from the RCSB Protein Data Bank (<http://www.rcsb.org/>, accessed on 10 September 2022).

### 2.3. Screening of Anthraquinone

The information on 70 anthraquinones was obtained from the Topscience database (<https://www.tsbiochem.com/>, accessed on 10 September 2022), seen in Supplementary Materials. All structural formulas of small molecules were downloaded from the PubChem database (<https://pubchem.ncbi.nlm.nih.gov/>, accessed on 10 September 2022).

### 2.4. Molecular Docking

All small molecules and the RIPK1 protein (PDB ID:5HX6) were loaded into the Discovery Studio (DS) 2019 software (version 4.5, Dassault Systems, Paris, France). First, the RIPK1 protein was pre-processed, and then, using the Macromolecules module, the pre-treated RIPK1 protein was identified as the receptor, and the docking activity pocket was determined. Before docking, AQs were processed with hydrogenation, charge, etc., using the Small Molecules module in DS. The reference ligand was necrostatin-1, a previously reported RIPK1 inhibitor. The LibDock module is used for preliminary screening. The docking results are sorted by docking score, Libscore, from high to low, and inhibitor candidates with a higher Libscore than necrostatin-1 were chosen. The DOCKTHOR web server was used to calculate ligand–receptor binding energy [15]. Based on the CHARMM force field, the CDOCKER module is used for semi-flexible docking. Analyses were conducted on the docking pattern between potential inhibitors and RIPK1 protein. Refer to previous reports for specific parameter settings [16,17].

### 2.5. ADMET Prediction and Pharmacological Analysis

The ADME (absorption, distribution, metabolism, and excretion) properties of the candidate inhibitors were analyzed using the ADME module of the DS 2019 software. Hepatotoxicity is a significant safety issue for medication developers, regulators, and doctors. The ProTox-II web server [18] was used to analyze the toxicity of the candidate inhibitors. In brief, data from the DILIrank [19] and NIH LiverTox [20] databases support ProTox-II 's prediction of hepatotoxicity. In addition, the ProTox-II web server makes predictions for carcinogenicity, immunotoxicity, mutagenicity, and cytotoxicity. The Feature mapping module of DS 2019 software was utilized to analyze the pharmacophore of necrostatin-1 and the candidate inhibitors, such as hydrophobic, hydrogen bond (HB) acceptor, HB-donor, positive ion, and ring aromatic.

### 2.6. Molecular Dynamics Simulation

For MD simulations, the optimal binding conformation of the AQs-RIPK1 complexes established by CDOCKER docking was used. Place the ligand/receptor complex in an orthorhombic box. Simulate a physiological milieu by adding sodium chloride to the system. Relax the system by minimizing the CHARMM force field's energy. Using analytical trajectory techniques, determine the root mean square deviation (RMSD), potential energy, and structural characteristics.

## 3. Results

### 3.1. Discrimination of Necroptosis-Related DEGs in AP

From the dataset GSE109227, 1631 AP-associated DEGs were identified, comprising 1333 genes with upregulation and 298 genes with downregulation (Figure 1A). The DEGs linked with AP intersected with necroptosis genes, and the resulting data was shown on a Venn diagram. Twelve genes that overlapped were found (Figure 1B). After importing the PPI data from the STRING database into the Cytoscape software (version 3.8.2, the National Institute of General Medical Sciences, Bethesda, MD, USA), the following proteins

were chosen to plot the PPI network based on their degree values: BNIP3, EGFR, HSPA4, HSP90AA1, MLKL, RIPK1, RNF31, SQSTM1, STAT3, TARDBP, and TNFRSF1A. This is depicted in Figure 1C. Based on the node degree and the biological function, RIPK1 was found to be the necroptosis-related gene of AP that was considered to be the most important. Figure 1D shows the relative expression levels of RIPK1 that were found in the control sample as well as the AP sample.

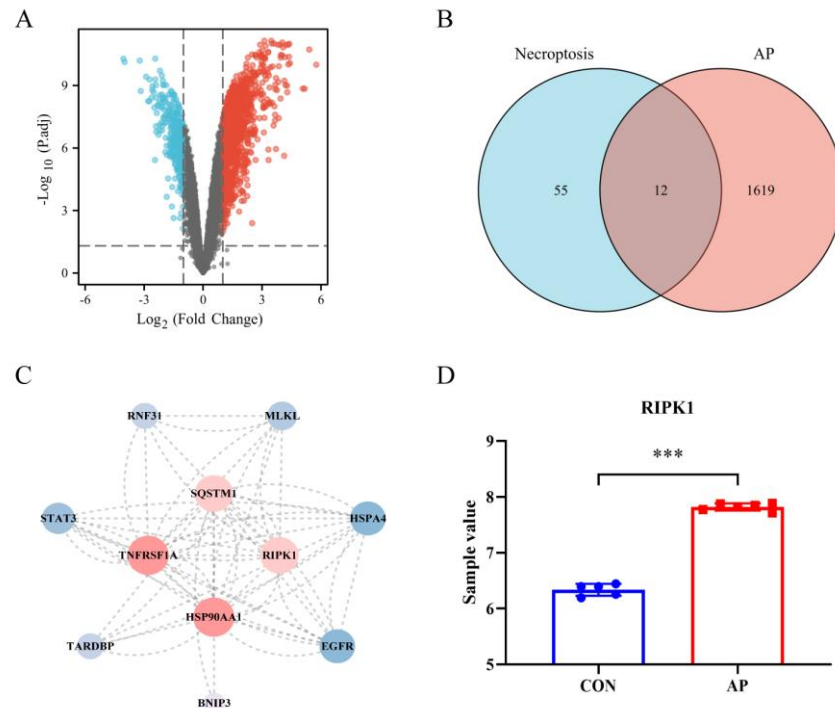


**Figure 1.** Discrimination of necroptosis-related DEGs in AP. (A) Volcano plot of DEGs among GSE109227 datasets; (B) Venn diagram of AP and necroptosis; (C) Protein-protein interaction network; (D) Relative expression of RIPK1 in control samples and AP samples. Red nodes in A are up-regulated genes; blue nodes in A are down-regulated genes; \*\*\*,  $p < 0.001$ ; red nodes in D are the AP group sample; blue nodes in D are the CON group sample.

### 3.2. LibDock of Active Ingredients against RIPK1

70 AQs were taken from the Topscience database, and then loaded into the DS 2019 software to do fast molecular docking with RIPK1 using LibDock. 12 AQs could be docked with RIPK1. See Table 1 for a list of the 5 AQs had better docking scores with RIPK1 than necrostatin-1. Figure 2 displays their structures in 2D structures.

**Table 1.** LibDock scores of the six compounds.

Number	Compounds	LibDock Scores	Binding Energies (Kcal/mol)
1	Lucidin Primeveroside	164.697	−6.83
2	Aloe-Emodin-8-O-Beta-D-Glucopyranoside	148.133	−7.17
3	Torososide A	143.923	−6.91
4	Rheochrysin	122.628	−7.07
5	Carminic acid	121.766	−7.04
6	Necrostatin-1	111.152	−6.99

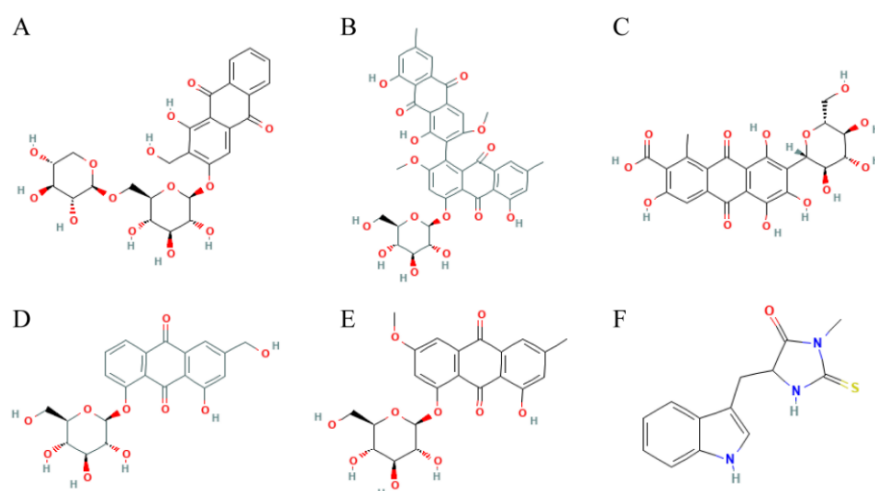


**Figure 2.** Structures of anthraquinone selected from virtual screening. (A) Lucidin Primeveroside; (B) Aloe-Emodin-8-O-Beta-D-Glucopyranoside; (C) Torososide A; (D) Rheochrysin; (E) Carminic acid; (F) Necrostatin-1.

### 3.3. ADME, and TOPKAT of Candidate Active Ingredients

Using the ADME module of the DS 2019 software, the pharmacological characteristics of the five potential small compounds and the reference ligand necrostatin-1 were analyzed (Table 2). Specifically, water solubility was shared by Aloe-Emodin-8-O-Beta-D-Glucopyranoside (A8G), Torososide A, Rheochrysin, and Carminic acid. Both Lucidin Primeveroside and necrostatin-1 showed a poor ability to dissolve in water. Necrostatin-1 demonstrated high levels of the blood-brain barrier (BBB). On the other hand, the BBB levels of A8G, torososide A, rheochrysin, carminic acid, and lucidin primeveroside were not well defined. Regarding inhibition of CYP2D6, none of the five candidate small molecules or necrostatin-1 are thought to have inhibitory effects. According to the predictions of the levels of intestinal absorption, the five compounds demonstrated extremely low intestinal absorption levels. Finally, all five compounds, as well as necrostatin-1, showed low levels of plasma protein binding (PPB).

**Table 2.** ADME of the five compounds and necrostatin-1.

Compounds	Solubility Level <sup>a</sup>	BBB Level <sup>b</sup>	CYP2D6 <sup>c</sup>	Absorption Level <sup>d</sup>	PPB Level <sup>e</sup>
Lucidin Primeveroside	2	4	0	3	0
Aloe-Emodin-8-O-Beta-D-Glucopyranoside	3	4	0	3	0
Torososide A	3	4	0	3	0
Rheochrysin	3	4	0	3	0
Carminic acid	3	4	0	3	0
Necrostatin-1	2	2	0	0	0

<sup>a</sup>: 0, Extremely low; 1, Very low, but possible; 2, Low; 3, Good; 4, Optimal; 5, Soluble. <sup>b</sup>: 0, Very high penetrant; 1, High; 2, Medium; 3, Low; 4, Undefined. <sup>c</sup>: 0, Non-inhibitor; 1, Inhibitor. <sup>d</sup>: 0, Good; 1, Moderate; 2, Low; 3, Very low. <sup>e</sup>: 0, Absorbent weak; 1, Absorbent strong.

One other thing we should be worried about is how safe the medications are. The online program ProTox-II was used to analyze the toxicity of five anthraquinones and necrostatin-1 (Table 3). All anthraquinones and necrostatin-1 were shown to be free of carcinogenic and cytotoxic properties. Both A8G and Torososide A were shown to have a harmful effect on the liver. Each of the five AQs exhibited immunotoxic properties. Lucidin primeveroside, rheochrysin, and carminic acid might be mutagenic. Rheochrysin and A8G were identified as potential inhibitors of RIPK1 based on the results of the molecular docking study in conjunction with those findings. Rheochrysin is a medication that belongs

to class 5 and has a lethal dose (LD 50) of 3000 mg/kg. The LD 50 of A8G is 1190 mg/kg body weight.

**Table 3.** Toxicity of the five compounds and necrostatin-1.

Compounds	LD50 (mg/kg)	Hepatotoxicity	Carcinogenicity	Immunotoxicity	Mutagenicity	Cytotoxicity
Lucidin Primeveroside	3000 (Class 5)	Inactive	Inactive	Active	Active	Inactive
Aloe-Emodin-8-O-Beta-D-Glucopyranoside	1190 (Class 4)	Active	Inactive	Active	Inactive	Inactive
Torososide A	1190 (Class 4)	Active	Inactive	Active	Inactive	Inactive
Rheochrysin	3000 (Class 5)	Inactive	Inactive	Active	Active	Inactive
Carminic acid	7 (Class 2)	Inactive	Inactive	Active	Active	Inactive
Necrostatin-1	200 (Class 3)	Inactive	Inactive	Inactive	Inactive	Inactive

### 3.4. Ligand Binding Analysis, Pharmacophore Analysis and Molecular Dynamics Simulation

Precise molecular docking of necrostatin-1 (Figure 3A), rheochrysin (Figure 4A), and A8G (Figure 5A) to RIPK1 were performed using the CDocker module. The CDocker interaction energy of rheochrysin and Aloe-Emodin-8-O-Beta-D-Glucopyranoside was higher than that of necrostatin-1, see Table 4. The hydrogen bond interaction and Pi-Pi-related interaction parameters between necrostatin-1, rheochrysin, A8G, and RIPK1 are shown in Tables 5 and 6. In molecular docking simulations, interactions between the receptor and ligand, such as hydrogen bonding, alkylation, and salt bridges, facilitate higher binding activity. According to the data, only three pairs of hydrogen bonds were formed in the necrostatin-1-RIPK1 complex. Eight pairs of hydrogen bonds were formed between rheochrysin and RIPK1. RIPK1 formed ten pairs of hydrogen bonds with A8G. Moreover, three Pi-alkyl interactions were formed between necrostatin-1 and RIPK1. With RIPK1, rheochrysin formed one pair of alkyl interactions and two pairs of Pi interactions, including Pi-Pi and Pi-alkyl interactions. Three pairs of Pi interactions were formed between A8G and RIPK1, including Pi-Pi and Pi-alkyl interactions. Compared to necrostatin-1, the increased number of hydrogen bonds and  $\pi$ -related interactions enhanced the affinity and stability of the interaction between the selected Aqs and RIPK1.

**Table 4.** CDocker potential energy of three compounds with RIPK1.

Compounds	CDocker Interaction Energy (kcal/mol)
Aloe-Emodin-8-O-Beta-D-Glucopyranoside	−55.1605
Rheochrysin	−52.2277
Necrostatin-1	−35.4412

**Table 5.** Hydrogen bond interaction parameters for compounds with RIPK1.

Compound	Donor Atom	Receptor Atom	Distances (Å)
Aloe-Emodin-8-O-Beta-D-Glucopyranoside	HIS72:HE	Aloe-Emodin-8-O-Beta-D-Glucopyranoside:O1	2.1
	HIS72:HE2	Aloe-Emodin-8-O-Beta-D-Glucopyranoside:O6	2.6
	ARG74:HE	Aloe-Emodin-8-O-Beta-D-Glucopyranoside:O4	2.9
	ARG74:HH21	Aloe-Emodin-8-O-Beta-D-Glucopyranoside:O4	2.5
	ARG286:HH22	Aloe-Emodin-8-O-Beta-D-Glucopyranoside:O5	2.8
	SER73:HN	Aloe-Emodin-8-O-Beta-D-Glucopyranoside:O7	2.3

Table 5. Cont.

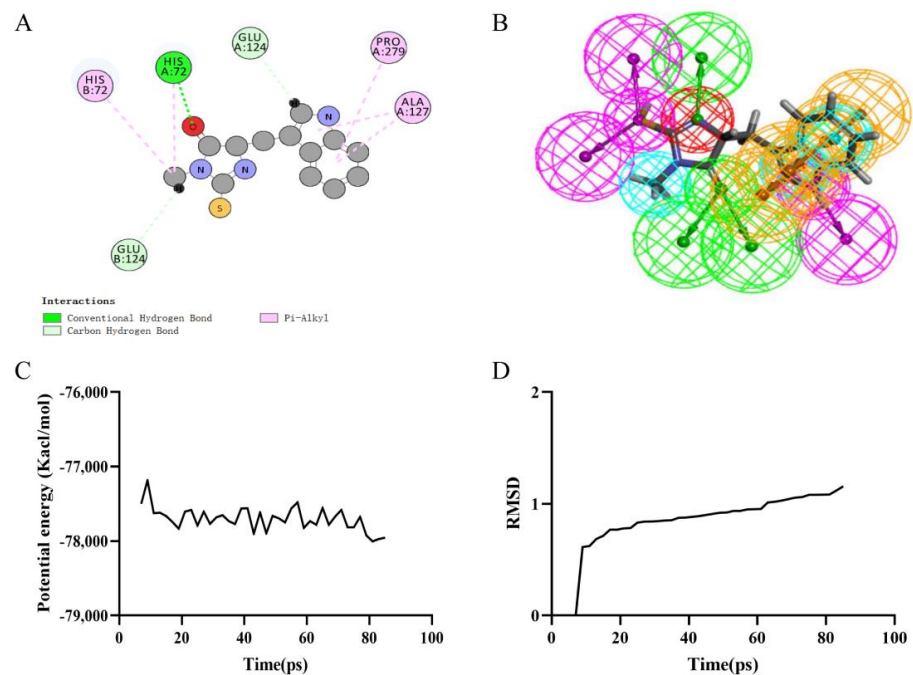
Compound	Donor Atom	Receptor Atom	Distances (Å)
Rheochrysin	ARG74:HE	Aloe-Emodin-8-O-Beta-D-Glucopyranoside:O3	3.0
	ARG74:HH21	Aloe-Emodin-8-O-Beta-D-Glucopyranoside:O3	2.4
	Aloe-Emodin-8-O-Beta-D-Glucopyranoside:H32	GLU124:OE2	2.0
	Aloe-Emodin-8-O-Beta-D-Glucopyranoside:H33	GLU124:OE2	1.9
	Aloe-Emodin-8-O-Beta-D-Glucopyranoside:H36	GLU282:OE2	2.2
	Aloe-Emodin-8-O-Beta-D-Glucopyranoside:H37	PRO279:O	2.1
	SER73:HN	Rheochrysin:O6	2.6
	SER73:HG	Rheochrysin:O6	1.8
	LYS132:HZ3	Rheochrysin:O9	3.0
	Rheochrysin:H35	GLU282:OE2	2.7
	Rheochrysin:H37	GLU282:OE1	2.6
	Rheochrysin:H38	GLU124:OE2	2.3
	Rheochrysin:H39	GLU124:OE2	2.4
	Rheochrysin:H44	GLU124:OE2	2.7
	Rheochrysin:H36	HIS72	2.4
Necrostatin-1	HIS72:HE2	Necrostatin-1:O2	2.1
	Necrostatin-1:H24	GLU124:O	2.6
	Necrostatin-1:H26	GLU124:OE2	3.0

Table 6. Pi-Pi staked interaction, Pi-Alkyl interaction, and Pi-Pi T-shaped interaction parameters for compounds with RIPK1.

Interaction Parameters	Compound	Donor Atom	Receptor Atom	Distances (Å)
Pi-Pi staked interaction	Aloe-Emodin-8-O-Beta-D-Glucopyranoside	HIS72	Aloe-Emodin-8-O-Beta-D-Glucopyranoside	5.3
Pi-Alkyl interaction		Aloe-Emodin-8-O-Beta-D-Glucopyranoside	ALA127	4.9
		Aloe-Emodin-8-O-Beta-D-Glucopyranoside	ARG71	4.8
Pi-Pi T-shaped interaction	Rheochrysin	HIS72	Rheochrysin	5.5
Pi-Alkyl interaction		Rheochrysin:C31	PRO279	4.9
		Rheochrysin:C31	ARG71	4.1
Pi-Alkyl interaction	Necrostatin-1	HIS72	Necrostatin-1:C15	4.8
		Necrostatin-1	ALA127	4.1
		Necrostatin-1	PRO279	5.4

Based on the assessment of the pharmacophore models by the Feature Mapping module, necrostatin-1 showed five HB-acceptors, three hydrogen donors, three hydrophobics, and one positive ion, respectively, as well as four ring aromatics (Figure 3B). Rheochrysin showed 27 HB-acceptors, 19 hydrogen donors, three hydrophobics, and two ring aromatics, respectively (Figure 4B). In addition, A8G showed 29 HB-acceptors, 25 hydrogen donors, two hydrophobics, and four ring aromatics, respectively (Figure 5B).

The molecular dynamics simulation module was used to assess the stability of the ligand-RIPK1 complex in its natural environment. The results show that the RMSD and potential energy of the complexes stabilize over time (Figures 3C,D–5C,D).



**Figure 3.** Ligand binding analysis, pharmacophore analysis and molecular dynamics simulation of Necrostatin-1. (A) 2D diagram of inter-molecular interaction of Necrostatin-1 with RIPK1; (B) Pharmacophore predictions of Necrostatin-1; green represents hydrogen acceptor; blue represents the hydrophobic center; purple represents hydrogen donor; red represents inozable positive; yellow represents aromatic ring by Schrodinger. (C) Potential Energy by MD simulations of Necrostatin-1; (D) Average backbone RMSD of MD simulations to Necrostatin-1.

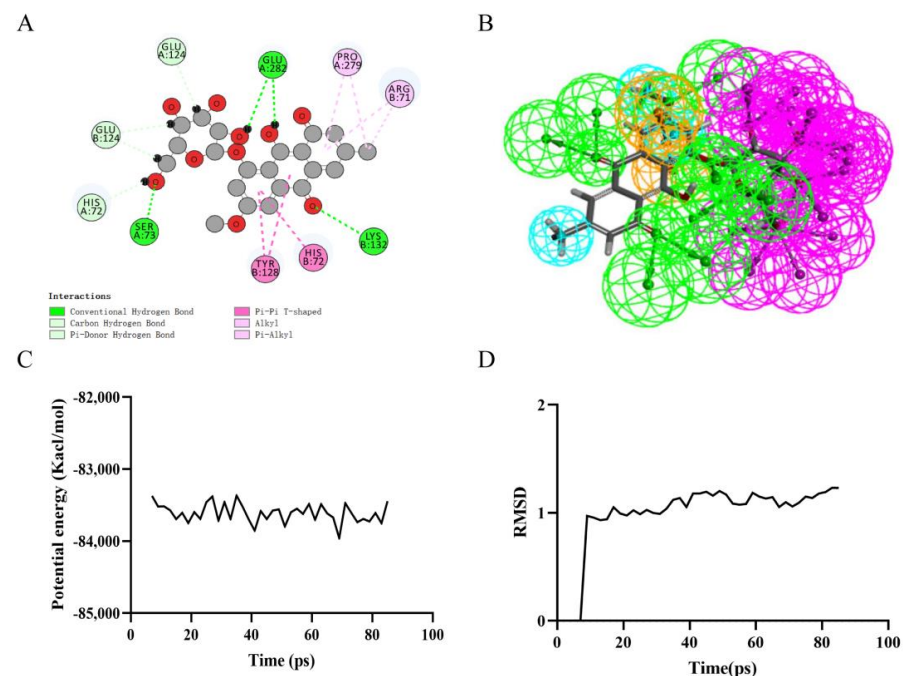


**Figure 4.** Ligand binding analysis, pharmacophore analysis and molecular dynamics simulation of Rheochrysin. (A) 2D diagram of inter-molecular interaction of Rheochrysin with RIPK1; (B) Pharmacophore predictions; green represents hydrogen acceptor; blue represents the hydrophobic center; purple represents hydrogen donor; yellow represents aromatic ring by Schrodinger. (C) Potential Energy; (D) Average backbone RMSD.

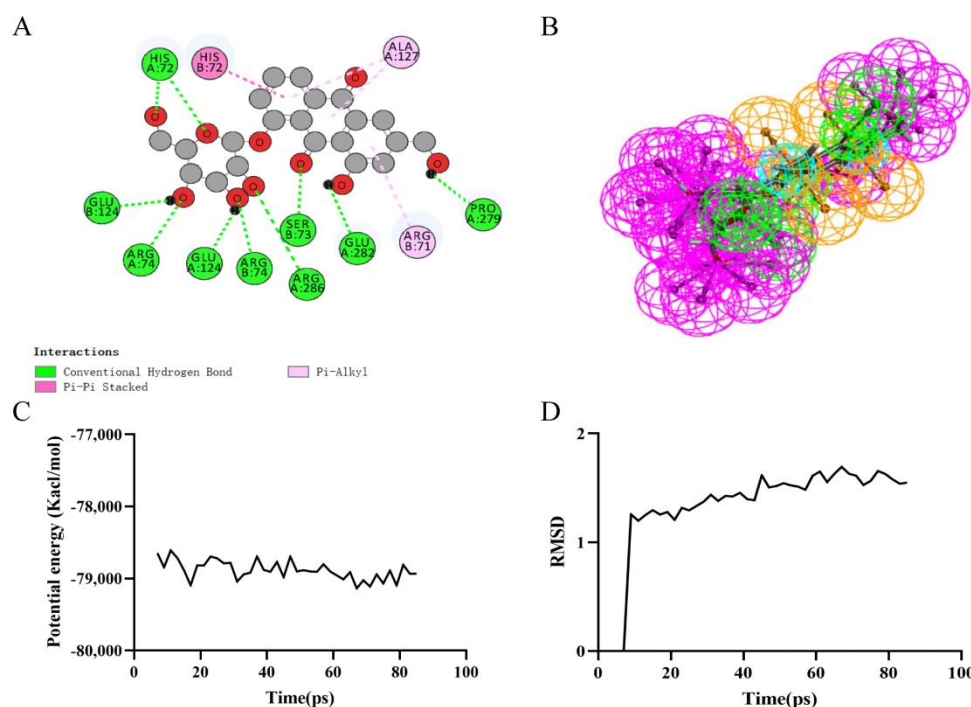


**Figure 5.** Ligand binding analysis, pharmacophore analysis and molecular dynamics simulation of Aloe-Emodin-8-O-Beta-D-Glucopyranoside. (A) 2D diagram of inter-molecular interaction of Aloe-Emodin-8-O-Beta-D-Glucopyranoside with RIPK1; (B) Pharmacophore predictions; green represents hydrogen acceptor; blue represents the hydrophobic center; purple represents hydrogen donor; yellow represents aromatic ring by Schrodinger. (C) Potential Energy; (D) Average backbone RMSD.

#### 4. Discussion

AP is one of the most common clinical abdominal emergencies with complex pathogenesis and high morbidity and mortality. There are no specific drugs available for SAP. In recent years, cell death-based therapeutic strategies have evolved rapidly. Necroptosis is a novel form of regulated cell necrosis, and its relationship with the severity and prognosis of AP has attracted growing interest [21,22]. Signals delivered by death receptors, such as tumor necrosis factor- $\alpha$  receptor 1 (TNFR1) induce phosphorylation of RIPK1 and RIPK3, and phosphorylated RIPK3 recruits and phosphorylates MLKL, leading to its translocation to the plasma membrane and ultimately to cell rupture and death. Inhibition of RIPK3 or lack of MLKL has been reported to significantly attenuate autophagy-related genes 7 deletion and caerulein-induced pancreatic injury [23,24]. Similarly, suppression of necroptosis with necrostatin-1 (the RIPK1 inhibitor) could ameliorate the severity of acute pancreatitis [25]. Thus, the identification of drugs that target necroptosis is essential for the treatment of SAP.

Although research on RIPK1 inhibitors has continued for some years, none have been licensed for commercialization. Necrostatin-1 was found to be the first RIPK1 inhibitor. Available data suggest that necrostatin-1 protects mice and rats from inflammatory and central nervous system illnesses by inhibiting RIPK1-mediated necroptosis [26–28]. Necrostatin-1 has been shown to protect rodents, such as rats and mice, against AP. Inhibiting necrosis in pancreatic acinar cells was the precise mechanism through which necrostatin-1 ameliorated SAP [29]. Additional data showed that necrostatin-1 might inhibit acinar cell necrosis and reduce inflammation-induced tissue damage by inhibiting the RIPK1/nuclear factor kappa B (NF- $\kappa$ B) signaling pathway, a well-known inflammation amplifier [30]. Furthermore, necrostatin-1 prevented further damage to the mouse pancreas by reducing the production of reactive oxygen species during AP, thereby reducing the injury's severity [31]. However, necrostatin-1 is susceptible to metabolic instability and targets indoleamine-2,3-dioxygenase, which may promote tumor immunological tolerance [32].

Also, necrostatin-1 blocks other forms of programmed cell death, including ferroptosis, raising questions about the molecule's selectivity [33]. Several RIPK1 inhibitors, including GSK2982772, SAR443122, SAR443820, GFH312, DNL758, and R552, have entered clinical trials for psoriasis, multiple sclerosis, and systemic lupus erythematosus [34]. Other clinical trials of RIPK1 inhibitors, GSK3145095 and DNL747, have been halted [34]. Furthermore, multiple FDA-approved pharmaceuticals have been evaluated for their capacity to inhibit RIPK1. Riebeling and colleagues discovered primidone, an aromatic antiepileptic medication, was a potent RIPK1 inhibitor to reduce necroptosis and inflammatory responses in systemic inflammatory response syndrome mice [35]. In a nutshell, scientists are still interested in finding RIPK1 inhibitors with better activity and selectivity.

The usage of DS 2019 software for virtual screening was the primary focus of this investigation. The LibDock program was used to conduct the first screening for ligands that might bind to RIPK1 after the initial download of 70 anthraquinones from Pubchem as a small molecule database. According to the findings, 12 different ligands were successful in forming strong bonds with the RIPK1 crystal structure. Based on their LibDock score, the top five ligands were chosen for further investigation. Rheochrysin and A8G were the two candidate anthraquinones that were further identified by pharmacological and toxicity profiling. The CDOCKER module was used to verify whether or not the two anthraquinones could bind to RIPK1 and to analyze their docking Potential Energy with RIPK1. According to the findings, the binding potentials of A8G and rheochrysin to RIPK1 were much greater than those of necrostatin-1. In addition, the hydrogen bonds,  $\pi$ -related interactions, and pharmacodynamic groups of these two AQs were compared to necrostatin-1. A8G and rheochrysin had a greater propensity for binding to RIPK1 than necrostatin-1. MD simulations were run to verify the stability of the ligand–receptor complexes by running RMSD and calculating the potential energy. The calculations show that the three ligand-RIPK1 complexes can reach equilibrium in a short period under natural conditions and stabilize over time.

Rheochrysin, also known as physcion-8-O-beta-D-glucoside, is an anthraquinone glycoside found in *Fallopia multiflora*, *Saururus Chinensis*, *Rheum australe*, *Selaginella delicatula*, and *Cortinarius canarius* [36]. Rheochrysin shows significant anti-inflammatory, antioxidant, hypolipidemic, and antitumor properties. According to recent research, different doses of rheochrysin prevented the entrance of phosphorylated NF- $\kappa$ B into the nucleus [37]. NF- $\kappa$ B is a recognized amplifier of the inflammatory signaling pathway and plays a crucial role in the AP-mediated necroptosis cascade response [38]. Aloe-Emodin-8-O-beta-D-glucopyranoside (A8G) is an analogue of emodin found in *Rheum officinale*, *Senna alexandrina*, and *Saussurea lappa* [39]. A8G is a moderate inhibitor of the human protein tyrosine phosphatase 1B (PTP1B) [40]. According to available evidence, cerulein-induced mild AP is related to elevated PTP1B protein expression [41]. Therefore, A8G has therapeutic promise for AP. In addition, several studies have shown that rhubarb and *Polygonum cuspidatum* contain much more A8G than free AQs, such as emodin [42,43]. Emodin is a well-studied free AQ with protective properties against AP-induced acinar cell damage, systemic inflammatory response, and organ damage [44,45].

In a word, this research takes a first step toward developing RIPK1 inhibitors by screening AQs that have the potential to be more effective than the reference ligand necrostatin-1. Still, there are gaps in this research that need to be filled. On the one hand, additional *in vivo* and *in vitro* experiments are required to verify the activity and safety of the selected AQs. Our research will concentrate on these areas. It is also important to note that the two AQs we selected are not perfect and have room for improvement or modification.

## 5. Conclusions

Based on the GEO and GSEA databases, this work identified RIPK1 as the most critical gene in AP-related necroptosis events. Computational-assisted drug analysis approaches were then utilized to screen anthraquinones for compounds that may operate specifically as RIPK1 inhibitors. Molecular docking, pharmacological characterization, toxicity analysis,

pharmacophore prediction, and molecular dynamics simulations utilizing DS 2019 software and website found rheochrysin and Aloe-Emodin-8-O-D-Glucopyranoside as possible new RIPK1 inhibitors. We present prospective leads for further preclinical research and investigations on these two anthraquinones.

**Supplementary Materials:** The following supporting information can be downloaded at: <https://www.mdpi.com/article/10.3390/pr10112260/s1>, Table S1: Necroptosis-related genes from the GSEA database. Table S2: Acute pancreatitis-related differentially expressed genes from the GSE109227 gene set. Table S3: Anthraquinone database.

**Author Contributions:** Conceptualization, Q.W. and H.C.; methodology, J.Y.; software, Y.L. (Yalan Luo); validation, X.L., Y.L. (Yan Liu) and Y.W.; data curation, J.Y.; writing—original draft preparation, Y.L.; writing—review and editing, J.Y. and P.W.; project administration, Q.W.; funding acquisition, H.C. All authors have read and agreed to the published version of the manuscript.

**Funding:** This study received no external funding.

**Conflicts of Interest:** The authors declare no conflict of interest.

## References

1. Boxhoorn, L.; Voermans, R.P.; Bouwense, S.A.; Bruno, M.J.; Verdonk, R.C.; Boermeester, M.A.; van Santvoort, H.C.; Besselink, M.G. Acute pancreatitis. *Lancet* **2020**, *396*, 726–734. [[CrossRef](#)]
2. Ge, P.; Luo, Y.; Okoye, C.S.; Chen, H.; Liu, J.; Zhang, G.; Xu, C.; Chen, H. Intestinal barrier damage, systemic inflammatory response syndrome, and acute lung injury: A troublesome trio for acute pancreatitis. *Biomed. Pharmacother. Biomed. Pharm.* **2020**, *132*, 110770. [[CrossRef](#)] [[PubMed](#)]
3. Wang, G.; Qu, F.Z.; Li, L.; Lv, J.C.; Sun, B. Necroptosis: A potential, promising target and switch in acute pancreatitis. *Apoptosis* **2016**, *21*, 121–129. [[CrossRef](#)] [[PubMed](#)]
4. Ju, E.; Park, K.A.; Shen, H.M.; Hur, G.M. The resurrection of RIP kinase 1 as an early cell death checkpoint regulator—a potential target for therapy in the necroptosis era. *Exp. Mol. Med.* **2022**, *54*, 1401–1411. [[CrossRef](#)] [[PubMed](#)]
5. Weinlich, R.; Oberst, A.; Beere, H.M.; Green, D.R. Necroptosis in development, inflammation and disease. *Nat. Rev. Mol. Cell Biol.* **2017**, *18*, 127–136. [[CrossRef](#)]
6. Vandenabeele, P.; Galluzzi, L.; Vanden Berghe, T.; Kroemer, G. Molecular mechanisms of necroptosis: An ordered cellular explosion. *Nat. Rev. Mol. Cell Biol.* **2010**, *11*, 700–714. [[CrossRef](#)]
7. He, R.; Wang, Z.; Dong, S.; Chen, Z.; Zhou, W. Understanding Necroptosis in Pancreatic Diseases. *Biomolecules* **2022**, *12*, 828. [[CrossRef](#)]
8. Deane, C.; Mokaya, M. A virtual drug-screening approach to conquer huge chemical libraries. *Nature* **2022**, *601*, 322–323. [[CrossRef](#)]
9. van Os, F.H. Some aspects of the pharmacology of anthraquinone drugs. *Pharmacology* **1976**, *14* (Suppl. 1), 18–29. [[CrossRef](#)]
10. Zhou, Q.; Xiang, H.; Liu, H.; Qi, B.; Shi, X.; Guo, W.; Zou, J.; Wan, X.; Wu, W.; Wang, Z.; et al. Emodin Alleviates Intestinal Barrier Dysfunction by Inhibiting Apoptosis and Regulating the Immune Response in Severe Acute Pancreatitis. *Pancreas* **2021**, *50*, 1202–1211. [[CrossRef](#)]
11. Xu, C.; Luo, Y.; Ntim, M.; Quan, W.; Li, Z.; Xu, Q.; Jiang, L.; Zhang, J.; Shang, D.; Li, L.; et al. Effect of emodin on long non-coding RNA-mRNA networks in rats with severe acute pancreatitis-induced acute lung injury. *J. Cell. Mol. Med.* **2021**, *25*, 1851–1866. [[CrossRef](#)] [[PubMed](#)]
12. Xu, C.; Zhang, J.; Liu, J.; Li, Z.; Liu, Z.; Luo, Y.; Xu, Q.; Wang, M.; Zhang, G.; Wang, F.; et al. Proteomic analysis reveals the protective effects of emodin on severe acute pancreatitis induced lung injury by inhibiting neutrophil proteases activity. *J. Proteom.* **2020**, *220*, 103760. [[CrossRef](#)] [[PubMed](#)]
13. Xia, S.; Ni, Y.; Zhou, Q.; Liu, H.; Xiang, H.; Sui, H.; Shang, D. Emodin Attenuates Severe Acute Pancreatitis via Antioxidant and Anti-inflammatory Activity. *Inflammation* **2019**, *42*, 2129–2138. [[CrossRef](#)] [[PubMed](#)]
14. Han, X.A.; Jie, H.Y.; Wang, J.H.; Zhang, X.M.; Wang, J.; Yu, C.X.; Zhang, J.L.; He, J.; Chen, J.Q.; Lai, K.F.; et al. Necrostatin-1 Ameliorates Neutrophilic Inflammation in Asthma by Suppressing MLKL Phosphorylation to Inhibiting NETs Release. *Front. Immunol.* **2020**, *11*, 666. [[CrossRef](#)]
15. Guedes, I.A.; Costa, L.; Dos Santos, K.B.; Karl, A.; Rocha, G.K.; Teixeira, I.M.; Galheigo, M.M.; Medeiros, V.; Krempser, E.; Custódio, F.L.; et al. Drug design and repurposing with DockThor-VS web server focusing on SARS-CoV-2 therapeutic targets and their non-synonym variants. *Sci. Rep.* **2021**, *11*, 5543. [[CrossRef](#)]
16. Liu, N.; Wang, X.; Zhu, Z.; Li, D.; Lv, X.; Chen, Y.; Xie, H.; Guo, Z.; Song, D. Selected ideal natural ligand against TNBC by inhibiting CDC20, using bioinformatics and molecular biology. *Aging* **2021**, *13*, 23702–23725. [[CrossRef](#)]
17. Luo, Y.; Ge, P.; Wen, H.; Zhang, Y.; Liu, J.; Dong, X.; Lan, B.; Zhang, G.; Yang, Q.; Chen, H. C/EBP $\beta$  Promotes LPS-Induced IL-1 $\beta$  Transcription and Secretion in Alveolar Macrophages via NOD2 Signaling. *J. Inflamm. Res.* **2022**, *15*, 5247–5263. [[CrossRef](#)]

18. Banerjee, P.; Eckert, A.O.; Schrey, A.K.; Preissner, R. ProTox-II: A webserver for the prediction of toxicity of chemicals. *Nucleic Acids Res.* **2018**, *46*, W257–W263. [CrossRef]
19. Chen, M.; Suzuki, A.; Thakkar, S.; Yu, K.; Hu, C.; Tong, W. DILIrank: The largest reference drug list ranked by the risk for developing drug-induced liver injury in humans. *Drug Discov. Today* **2016**, *21*, 648–653. [CrossRef]
20. Thakkar, S.; Chen, M.; Fang, H.; Liu, Z.; Roberts, R.; Tong, W. The Liver Toxicity Knowledge Base (LKTb) and drug-induced liver injury (DILI) classification for assessment of human liver injury. *Expert Rev. Gastroenterol. Hepatol.* **2018**, *12*, 31–38. [CrossRef]
21. Mattia, G.; Puglisi, R.; Ascione, B.; Malorni, W.; Carè, A.; Matarrese, P. Cell death-based treatments of melanoma: conventional treatments and new therapeutic strategies. *Cell Death Dis.* **2018**, *9*, 112. [CrossRef] [PubMed]
22. Baig, S.; Seevasant, I.; Mohamad, J.; Mukheem, A.; Huri, H.Z.; Kamarul, T. Potential of apoptotic pathway-targeted cancer therapeutic research: Where do we stand. *Cell Death Dis.* **2016**, *7*, e2058. [CrossRef] [PubMed]
23. Wu, J.; Huang, Z.; Ren, J.; Zhang, Z.; He, P.; Li, Y.; Ma, J.; Chen, W.; Zhang, Y.; Zhou, X.; et al. Mkl1 knockout mice demonstrate the indispensable role of Mkl1 in necroptosis. *Cell. Res.* **2013**, *23*, 994–1006. [CrossRef]
24. Zhou, X.; Xie, L.; Xia, L.; Bergmann, F.; Büchler, M.W.; Kroemer, G.; Hackert, T.; Fortunato, F. RIP3 attenuates the pancreatic damage induced by deletion of ATG7. *Cell Death Dis.* **2017**, *8*, e2918. [CrossRef]
25. Louhimo, J.; Steer, M.L.; Perides, G. Necroptosis Is an Important Severity Determinant and Potential Therapeutic Target in Experimental Severe Pancreatitis. *Cell. Mol. Gastroenterol. Hepatol.* **2016**, *2*, 519–535. [CrossRef] [PubMed]
26. Dong, L.; Liang, F.; Lou, Z.; Li, Y.; Li, J.; Chen, Y.; Ding, J.; Jiang, B.; Wu, C.; Yu, H.; et al. Necrostatin-1 Alleviates Lung Ischemia-Reperfusion Injury via Inhibiting Necroptosis and Apoptosis of Lung Epithelial Cells. *Cells* **2022**, *11*, 3139. [CrossRef] [PubMed]
27. Liu, C.; Cao, Y.; Wang, H.X.; Zhao, L.; Chen, Y.X.; Zhong, K.H.; Li, G.W.; Wang, G.Q.; Huang, K.R.; Tong, A.P.; et al. Necrostatin-1 decreases necroptosis and inflammatory markers after intraventricular hemorrhage in mice. *Neural Regen. Res.* **2022**, *17*, 2710–2716. [CrossRef] [PubMed]
28. Yin, C.; Zhang, Q.; Zhao, J.; Li, Y.; Yu, J.; Li, W.; Wang, Q. Necrostatin-1 Against Sevoflurane-Induced Cognitive Dysfunction Involves Activation of BDNF/TrkB Pathway and Inhibition of Necroptosis in Aged Rats. *Neurochem. Res.* **2022**, *47*, 1060–1072. [CrossRef]
29. Song, G.; Ma, Z.; Liu, D.; Zhou, J.; Meng, H.; Zhou, B.; Qian, D.; Song, Z. Bone marrow-derived mesenchymal stem cells ameliorate severe acute pancreatitis by inhibiting necroptosis in rats. *Mol. Cell. Biochem.* **2019**, *459*, 7–19. [CrossRef]
30. Duan, P.Y.; Ma, Y.; Li, X.N.; Qu, F.Z.; Ji, L.; Guo, X.Y.; Zhang, W.J.; Xiao, F.; Li, L.; Hu, J.S.; et al. Inhibition of RIPK1-dependent regulated acinar cell necrosis provides protection against acute pancreatitis via the RIPK1/NF- $\kappa$ B/AQP8 pathway. *Exp. Mol. Med.* **2019**, *51*, 1–17. [CrossRef]
31. Ouyang, Y.; Wen, L.; Armstrong, J.A.; Chvanov, M.; Latawiec, D.; Cai, W.; Awais, M.; Mukherjee, R.; Huang, W.; Gough, P.J.; et al. Protective Effects of Necrostatin-1 in Acute Pancreatitis: Partial Involvement of Receptor Interacting Protein Kinase 1. *Cells* **2021**, *10*, 1035. [CrossRef] [PubMed]
32. Takahashi, N.; Duprez, L.; Grootjans, S.; Cauwels, A.; Nerinckx, W.; DuHadaway, J.B.; Goossens, V.; Roelandt, R.; Van Hauwermeiren, F.; Libert, C.; et al. Necrostatin-1 analogues: Critical issues on the specificity, activity and in vivo use in experimental disease models. *Cell Death Dis.* **2012**, *3*, e437. [CrossRef] [PubMed]
33. Friedmann Angeli, J.P.; Schneider, M.; Proneth, B.; Tyurina, Y.Y.; Tyurin, V.A.; Hammond, V.J.; Herbach, N.; Aichler, M.; Walch, A.; Eggenhofer, E.; et al. Inactivation of the ferroptosis regulator Gpx4 triggers acute renal failure in mice. *Nat. Cell Biol.* **2014**, *16*, 1180–1191. [CrossRef]
34. Clinical Trials Database. Available online: <https://clinicaltrials.gov> (accessed on 22 October 2022).
35. Riebeling, T.; Jamal, K.; Wilson, R.; Kolbrink, B.; von Samson-Himmelstjerna, F.A.; Moerke, C.; Ramos Garcia, L.; Dahlke, E.; Michels, F.; Lühder, F.; et al. Primidone blocks RIPK1-driven cell death and inflammation. *Cell Death Differ.* **2021**, *28*, 1610–1626. [CrossRef] [PubMed]
36. Yan, H.J.; Fang, Z.J.; Fu, J.; Yu, S.X. The correlation between bioactive components of Fallopia multiflora root and environmental factors. *Am. J. Chin. Med.* **2010**, *38*, 473–483. [CrossRef] [PubMed]
37. Li, X.; He, Y.; Wei, L.; Zhang, J.; Li, X.; Cui, W.; Zhang, S. Physcion-8-O- $\beta$ -d-glucoside interferes with the nuclear factor- $\kappa$ B pathway and downregulates P-glycoprotein expression to reduce paclitaxel resistance in ovarian cancer cells. *J. Pharm. Pharmacol.* **2021**, *73*, 545–552. [CrossRef]
38. Wang, X.; Zhang, L.; Li, P.; Zheng, Y.; Yang, Y.; Ji, S. Apelin/APJ system in inflammation. *Int. Immunopharmacol.* **2022**, *109*, 108822. [CrossRef]
39. Chen, A.; Sun, L.; Yuan, H.; Wu, A.; Lu, J.; Ma, S. Simultaneous qualitative and quantitative analysis of 11 active compounds in rhubarb using two reference substances by UHPLC. *J. Sep. Sci.* **2018**, *41*, 3686–3696. [CrossRef]
40. Li, S.; An, T.Y.; Li, J.; Shen, Q.; Lou, F.C.; Hu, L.H. PTP1B inhibitors from Saussurea lappa. *J. Asian. Nat. Prod. Res.* **2006**, *8*, 281–286. [CrossRef]
41. Sarmiento, N.; Sánchez-Bernal, C.; Pérez, N.; Sardina, J.L.; Mangas, A.; Calvo, J.J.; Sánchez-Yagüe, J. Rolipram and SP600125 suppress the early increase in PTP1B expression during cerulein-induced pancreatitis in rats. *Pancreas* **2010**, *39*, 639–645. [CrossRef]
42. Komatsu, K.; Nagayama, Y.; Tanaka, K.; Ling, Y.; Basnet, P.; Meselhy, M.R. Development of a high performance liquid chromatographic method for systematic quantitative analysis of chemical constituents in rhubarb. *Chem. Pharm. Bull.* **2006**, *54*, 941–947. [CrossRef] [PubMed]

43. Peng, W.; Qin, R.; Li, X.; Zhou, H. Botany, phytochemistry, pharmacology, and potential application of *Polygonum cuspidatum* Sieb. et Zucc.: A review. *J. Ethnopharmacol.* **2013**, *148*, 729–745. [[CrossRef](#)] [[PubMed](#)]
44. Cui, Y.; Chen, L.J.; Huang, T.; Ying, J.Q.; Li, J. The pharmacology, toxicology and therapeutic potential of anthraquinone derivative emodin. *Chin. J. Nat. Med.* **2020**, *18*, 425–435. [[CrossRef](#)]
45. Li, J.; Zhang, S.; Zhou, R.; Zhang, J.; Li, Z.F. Perspectives of traditional Chinese medicine in pancreas protection for acute pancreatitis. *World J. Gastroenterol.* **2017**, *23*, 3615–3623. [[CrossRef](#)] [[PubMed](#)]